Hydroelastic analysis of an axially loaded compliant fiber wetted with a droplet

Xiang-Fa Wu,[a] Amol Bedarkar, and Iskander S. Akhatov
Department of Mechanical Engineering, North Dakota State University, Fargo, North Dakota 58108-6050, USA

(Received 1 April 2010; accepted 5 August 2010; published online 25 October 2010)

Liquid droplets wetting on thin fibers induce appreciable capillary forces that may further modulate the mechanical behavior of the fibers, especially for those ultrathin compliant fibers made of polymeric materials (e.g., biopolymers, hydrogels, etc.). This paper aims to study the capillary effect in the mechanical response of an axially loaded compliant fiber wetted with droplets. First, the fiber is considered as a linearly elastic column and the critical condition of *Euler*-buckling due to a droplet wetting fiber, denoted as *capillary buckling*, is derived. Furthermore, a nonlinear continuum hydroelasticity model is formulated to examine the capillary effect in the mechanical response of an axially loaded compliant fiber wetted with a droplet. The fiber material is modeled as an incompressible, isotropic, hyperelastic Mooney–Rivlin solid. Barrel-shaped morphology of the droplet sitting on the fiber is assumed. Explicit hydroelastic solution to such a droplet-on-fiber system with large deformation is derived, which shows the dependency of mechanical response upon fiber diameter, droplet size, and surface wetting property of the system. Results show that in the case of hydrophilic fibers, capillary effect can enhance the load-carrying capacity of the thin fibers. The concepts and results presented in this study can be used to analyze the mechanical behavior of thin compliant fibers structured in wet and vapor-related environments (e.g., biological, colloid, and catalytic systems). © *2010 American Institute of Physics*. [doi:10.1063/1.3486471]

I. INTRODUCTION

Wetting and spreading of droplets on fibers and textiles is a ubiquitous microfluidic phenomenon that is commonly observed in life, scientific, and engineering activities (e.g., wetting of a spider web by morning dews, dyeing, cleaning, waterproof design of fabrics, etc.). Substantial progress has been made in understanding this intriguing process in the past several decades.[1–9] In particular, Carroll[10] first presented an elegant expression of barrel-shaped morphology of a microdroplet wetting on a fiber in term of Legendre's elliptical functions of the first and second kinds. Based on Carroll's theory,[10] quite a few updates[11–14] have been dedicated to facilitating the process of extracting the contact angle from droplet-on-fiber systems utilized in various experiments. In reality, a droplet sitting on a fiber can assume two exchangeable morphologies, i.e., the axisymmetric barrel-shaped morphology and the nonsymmetrical clamshell-shaped morphology, depending on the global potential energy of the droplet-on-fiber system at given fiber diameter, droplet volume and contact angle. By means of a surface finite element method,[15] Mchale *et al.*[16] and McHale and Newton[17] have identified the critical condition of morphology transition between a barrel-shaped droplet and a clamshell-shaped droplet wetting on a fiber in term of the critical droplet volume at varying contact angle. Similar morphology transition was also detected in the case of microdroplets suspending between parallel fibers.[18–20] In the special case of two parallel fibers of identical diameter and surface wetting properties, the related critical condition has been determined in terms of a family of characteristic wetting curves.[21,22] Such droplet-on-fiber systems are expected particularly useful to delivery of liquids of microliters and nanoliters.[23] In addition, when the two fibers are misaligned, symmetry breaking of the liquid droplet on the fibers will yield *capillary torque* as demonstrated in recent numerical experiments.[24,25] These in-depth studies have provided valuable knowledge helpful to understand and exploit a variety of droplet-on-fiber systems for practical applications including biological cell manipulation and development of microfluidic devices. It needs to mention that in the above studies, an implicit assumption has been adopted: the fibers were dealt with as stiff (rigid) rods and deformations due to capillary forces were neglected. Such an assumption can hold well for commonly used natural and synthetic fibers with the diameter over tens of microns since these fibers have sufficient elastic modulus and the capillary effect is not as significant as to induce appreciable elastic deformation of the fibers.

With recent progress in nanomanufacturing techniques, ultrathin compliant fibers (e.g., those amorphous biopolymer and hydrogel fibers) with the diameter of tens to hundreds of nanometers have been massively produced by electrospinning and other cutting-edge techniques.[26–30] Among others, compliant biopolymer nanofibers carrying targeted biochemical functions have been under intensive tests for potential therapy and other applications (e.g., tissue scaffolds and drug delivery) due to their high specific surface area, unique continuity, excellent biocompatibility, and easy structural and doping tailorability.[31–36] In practice, it is a common phenomenon that microdroplets wet and spread on these ultrathin fibers and fiber networks. For instance, vapor and liquids are

[a]Electronic mail: xiangfa.wu@ndsu.edu.

typically involved in the process of cultivating biological cells on filamentary scaffolds. To the best of authors' knowledge, no study has been reported yet on the mechanical behavior of compliant fibers involving capillary effect though such response can be considered as a kind of mild mechanical stimulus that can be tuned for biomedical applications.

In this study, we perform the hydroelastic analysis of an axially loaded compliant fibers wetted with liquid droplets. First, we examine the condition of capillary buckling that may happen in an ultrathin hydrophilic fiber owing to the capillary forces induced by a wetting droplet. To do so, concept of classic *Euler*-buckling of slender elastic columns will be adopted. Furthermore, a nonlinear continuum hydroelasticity model is formulated to examine the capillary effect in the mechanical response of an axially loaded compliant fiber wetted by a droplet. The fiber material is modeled as an incompressible, isotropic, hyperelastic Mooney–Rivlin solid; barrel-shaped morphology of the droplet is assumed. An explicit stress-stretch relationship of the wetted compliant fiber will be given. Numerical experiments will be demonstrated to examine the dependencies of mechanical behavior upon fiber diameter, elasticity, droplet size, and contact angle. Potential applications of the concepts and results obtained in this study will be further addressed in the end of the paper.

II. PROBLEM FORMULATION AND SOLUTION

A. Capillary buckling of thin fibers

Consider a straight thin fiber wetted by a liquid droplet. In this case, capillary effect appears in two ways, i.e., the capillary pressure acting on fiber surface and the axial compression (hydrophilic fiber) or tension (hydrophobic fiber) along the fiber axis, in which the former compresses the fiber while the latter stretches the fiber. For a droplet wetting on a hydrophilic fiber, the resulting axial compressive capillary force may, in general, trigger the classic *Euler*-type buckling of the fiber. In this fiber, we consider a straight segment fixed between two wetting fronts of the droplet, where the wetting length L may be determined using the droplet volume V_0 and the current fiber radius r_0 (to be discussed in Sec. II). The axial compressive force due to the droplet is:

$$F_{capillary} = 2\pi r_0 \gamma_{LV} \cos\theta, \tag{1}$$

where γ_{LV} is the surface tension of the liquid droplet and θ is the contact angle between the fiber material and the liquid droplet. The critical compressive force to trigger *Euler*-type buckling of a fixed elastic column of circular cross-section is[37]

$$F_c = \frac{4\pi^2 EI}{L^2}, \tag{2}$$

where E is the Young's modulus, and I is the area moment of fiber cross-section: $I=\pi r_0^4/4$. Substituting (1) into (2) yields the critical slenderness ratio λ_c (defined as L/r_0) such that

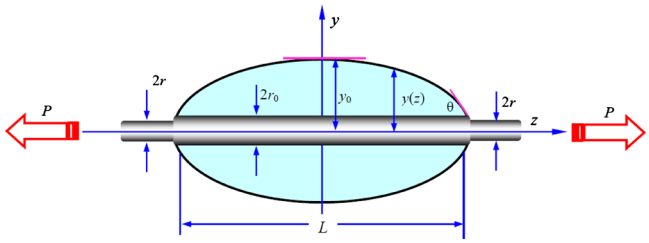

FIG. 1. (Color online) Geometries of a barrel-shaped droplet wetting on a thin compliant fiber subjected to axial stretch. In the diagram, r is the current fiber radius out of the droplet, and r_0 is the fiber radius within the droplet.

$$\lambda_{1c} = \pi\sqrt{\frac{Er_0}{2\gamma_{LV}\cos\theta}}. \tag{3}$$

In addition, by considering the fiber being jointed between the two wetting fronts, an alternative λ_c can be determined as[37]

$$\lambda_{2c} = \frac{\pi}{2}\sqrt{\frac{Er_0}{2\gamma_{LV}\cos\theta}}. \tag{4}$$

Thus, a reasonable value of λ_c to trigger capillary buckling of the thin fiber can be estimated as

$$\lambda_c \geq \pi\sqrt{\frac{Er_0}{2\gamma_{LV}\cos\theta}}. \tag{5}$$

To exemplify the value λ_c given by (5), consider a typical polymer microfiber of Young's modulus 10 GPa and diameter of 10 μm. Assume that the fiber is wetted by a water droplet (γ_{LV}=72.8 dyn/cm at 20 °C) with a contact angle θ=30°. The relation (5) gives the range of λ_c yielding capillary buckling as $\lambda_c > \sim 2\times 10^3$. This range is much larger than that formed by the wetting length of a common droplet. However, if selecting E=100 MPa and R_0=500 nm for an ultrathin compliant fiber, the range of λ_c for capillary buckling is $\lambda_c > \sim 45$, within a favorable range formed by a droplet. Thus, capillary buckling likely happens in ultrathin compliant fibers with the diameter below hundreds of nanometers such as those polymeric nanofibers produced by the low-cost electrospinning technique.[26–30]

B. Hydroelastic response of thin compliant fibers wetted with droplets

Let us further examine the capillary effect in the mechanical response of an axially loaded thin fiber wetted by a droplet. Now, the fiber is considered as a straight rod with circular cross-section and made of incompressible, isotropic, hyperelastic Mooney–Rivlin solid. In this case, the mechanical response of the fiber is combination of fiber elasticity and capillary forces induced by the droplet. Without loss of generality, hereafter we only consider the axial mechanical behavior of the fiber segment wetted by a droplet which assumes an axisymmetric barrel-shaped morphology,[10,14] as illustrated in Fig. 1. For a thin compliant fiber, finite radial deformation of the fiber can appear due to finite axial stretch and large capillary pressure exerted by the droplet. The final

configuration of the droplet-on-fiber system can be obtained through solving the hydroelastic problem involving nonlinear elasticity and capillary effect.

For an undisturbed stretch-free state, an imaginary configuration of the fiber (ignoring the droplet and fiber surface stress) is assumed to be a perfectly circular cylinder of initial radius R_0. Two configurations are adopted to describe the motion of a material point of the fiber, i.e., undisturbed stretch-free (without droplet and fiber surface stress) and current configuration (after deformation), respectively. The corresponding coordinates of the material point are denoted, respectively, by (R,Φ,Z) and (r,φ,z). To simplify the process, we only consider the deformation within the droplet and avoid the complicated phenomenon near the wetting fronts. In this case, deformation of the fiber segment is axisymmetric, independent of the location along the fiber axis:[38–42]

$$r=\lambda_1 R \quad (0\le R\le R_0), \quad \varphi=\Phi \quad (0\le\Phi\le 2\pi),$$
$$z=\lambda_3 Z \quad (-\infty\le Z\le+\infty), \tag{6}$$

where λ_1 and λ_3 are, respectively, the transverse and longitudinal stretches, independent of the spatial location within the droplet. Accordingly, the deformation gradient attached to the above deformation is

$$F=\begin{bmatrix} \frac{\partial r}{\partial R} & \frac{1}{R}\frac{\partial r}{\partial\Phi} & \frac{\partial r}{\partial Z} \\ r\frac{\partial\varphi}{\partial R} & \frac{r}{R}\frac{\partial\varphi}{\partial\Phi} & r\frac{\partial\varphi}{\partial Z} \\ \frac{\partial z}{\partial R} & \frac{1}{R}\frac{\partial z}{\partial\Phi} & \frac{\partial z}{\partial Z} \end{bmatrix}=\begin{bmatrix} \lambda_1 & 0 & 0 \\ 0 & \lambda_1 & 0 \\ 0 & 0 & \lambda_3 \end{bmatrix}. \tag{7}$$

Material incompressibility of the fiber material requires λ_1 and λ_3 satisfying

$$\lambda_1^2\lambda_3=1. \tag{8}$$

The left Cauchy–Green tensor $\mathbf{B}$ and its inverse can be expressed, respectively, as

$$\mathbf{B}=\mathbf{F}\mathbf{F}^{\mathbf{T}}=\mathrm{diag}[\lambda_1^2,\lambda_1^2,\lambda_3^2], \quad \mathbf{B}^{-1}=\mathrm{diag}[\lambda_1^{-2},\lambda_1^{-2},\lambda_3^{-2}]. \tag{9}$$

Furthermore, the scalar invariants of $\mathbf{B}$ are

$$I_1=2\lambda_1^2+\lambda_3^2=2\lambda_3^{-1}+\lambda_3^2, \quad I_2=2\lambda_3+\lambda_3^{-2}, \quad I_3=1. \tag{10}$$

In addition, the constitutive law of an incompressible, isotropic, hyperelastic Mooney–Rivlin solid can be expressed in terms of Cauchy stress tensor versus $\mathbf{B}$:[43]

$$\mathbf{T}=-p\mathbf{I}+2c_1\mathbf{B}-2c_2\mathbf{B}^{-1}, \tag{11}$$

where p is the hydrostatic pressure, c_1 and c_2 are two material parameters, and $\mathbf{I}$ is a unit tensor. In particular, when $c_2=0$ and c_1 being half the shear modulus, the material satisfying (11) is designated as neo-Hookean solid. In terms of stress components, the constitutive law (11) can be recast as

$$T_{rr}=T_{\varphi\varphi}=-p+2c_1\lambda_1^2-2c_2\lambda_1^{-2}=-p+2c_1\lambda_3^{-1}-2c_2\lambda_3, \tag{12}$$

$$T_{zz}=-p+2c_1\lambda_1^{-4}-2c_2\lambda_1^4=-p+2c_1\lambda_3^2-2c_2\lambda_3^{-2}, \tag{13}$$

$$T_{r\varphi}=T_{rz}=T_{\varphi z}=0. \tag{14}$$

In spatial cylindrical coordinates, equilibrium equations of the fiber are

$$\frac{\partial T_{rr}}{\partial r}+\frac{T_{rr}-T_{\varphi\varphi}}{r}=0, \tag{15}$$

$$\frac{\partial T_{\varphi\varphi}}{\partial\varphi}=0, \tag{16}$$

$$\frac{\partial T_{zz}}{\partial z}=0. \tag{17}$$

To determine the stress field of the fiber, two traction boundary conditions are needed. At the fiber surface, both interface energy and capillary effect of the droplet yield uniform radial compression:

$$T_{rr}=-\gamma_{LS}/r_0-p_c+2\gamma_{LV}\sin\theta/L. \tag{18}$$

In the above, the first term is the contribution of the compressive stress induced by the specific interface energy γ_{LS} (newton per meter) between the fiber and the liquid, in which γ_{LS} is assumed independent of the fiber radius and applied axial stretch λ_3 and r_0 is the current fiber radius after deformation; the second term is the contribution of capillary pressure p_c due to the droplet that can be determined by solving the resulting Young–Laplace equation;[10,14] the third term is the contribution of the capillary forces at the two wetting fronts which have been averaged over the wetting length. In addition, equation of force equilibrium along the fiber axis reads

$$P=2\pi\int_0^{r_0} rT_{zz}dr+2\pi r_0\gamma_{LV}\cos\theta, \tag{19}$$

where P is the external axial force. In the final equilibrium state, the surface traction T_{rr} in (18) is constant and therefore the above nonlinear elasticity problem can be solved explicitly.[39–42] Substituting Eqs. (12) and (13) into (16) and (17) leads to

$$\frac{\partial p}{\partial\varphi}=\frac{\partial p}{\partial z}=0. \tag{20}$$

The above relation indicates that the hydrostatic pressure p in the fiber segment is only a function with respect to r:

$$p=p(r). \tag{21}$$

By eliminating p in (12) and (13) and then using Eq. (18), the axial stress within the droplet can be determined as

$$T_{zz}=2\left(\lambda_3^2-\frac{1}{\lambda_3}\right)\left(c_1+\frac{c_2}{\lambda_3}\right)-\frac{\gamma_{LS}}{r_0}-p_c+\frac{2\gamma_{LV}\sin\theta}{L}. \tag{22}$$

Consequently, substitution of (22) into (19) yields the axial tension-stretch relationship as

$$P = 2\pi r_0^2\left(\lambda_3^2 - \frac{1}{\lambda_3}\right)\left(c_1 + \frac{c_2}{\lambda_3}\right) - \pi r_0\gamma_{LS} - \pi r_0^2 p_c + \frac{2\pi r_0^2\gamma_{LV}\sin\theta}{L} + 2\pi r_0\gamma_{LV}\cos\theta. \quad (23)$$

In the above, p_c can be determined by solving the hydrostatic problem of a barrel-shaped droplet wetting on a fiber of uniform cross-section (see Fig. 1). This problem can be formulated through minimizing the interfacial energy of the droplet:[14]

$$J = 4\pi\int_0^{L/2}\{(\gamma_{LS} - \gamma_{SV})r_0 + \gamma_{LV}y(z)\sqrt{1 + [y'(z)]^2}\}dz, \quad (24)$$

where L is the total wetting length of the droplet, $y(z)$ is the droplet radius at an arbitrary location z. Besides, in relation (24), symmetry of the droplet has been employed and gravity is ignored. The boundary conditions at $z=0$ (droplet mid-plane) and $z=L/2$ (wetting front) are

$$y'(0) = 0, \quad y(L/2) = r_0. \quad (25)$$

The unknown conditions include the peak radius y_0, i.e., $y(0)$, of the droplet at its symmetrical mid-plane and the fiber wetting length L, which can be determined through the constraint of constant droplet volume:

$$V_0 = 2\pi\int_0^{L/2}\{[y(z)]^2 - r_0^2\}dz. \quad (26)$$

Variation problem (24) under constraints (25) and (26) have been solved explicitly.[10,14] The resulting barrel-shaped morphology carries the form:

$$z = \int_y^{y_0}(y^2 + \eta r_0 y_0)/\sqrt{(y_0^2 - y^2)(y^2 - \eta^2 r_0^2)}dy, \quad (27)$$

where

$$\eta = (y_0\cos\theta - r_0)/(y_0 - r_0\cos\theta). \quad (28)$$

As a consequence, the capillary pressure p_c of the droplet is[10]

$$p_c = 2\gamma_{LV}(y_0 - r_0\cos\theta)/(y_0^2 - r_0^2). \quad (29)$$

With the aid of relation (27), the expression of the droplet volume (26) can be rewritten as

$$V_0 = 2\pi\int_{r_0}^{y_0}(y^2 - r_0^2)(y^2 + \eta r_0 y_0)/\sqrt{(y_0^2 - y^2)(y^2 - \eta^2 r_0^2)}dy. \quad (30)$$

Given a droplet of volume V_0 wetting on a fiber segment of current radius r_0, the droplet radius at the mid-plane y_0 can be determined from (30) by using a numerical scheme. Once y_0 is obtained, p_c can be determined from (29), and L can be found from (27) such that

$$L = 2\int_{r_0}^{y_0}(y^2 + \eta r_0 y_0)/\sqrt{(y_0^2 - y^2)(y^2 - \eta^2 r_0^2)}dy. \quad (31)$$

With relations (23) and $r_0=\lambda_1 R_0=R_0/\sqrt{\lambda_3}$, the axial engineering stress of the fiber within the droplet can expressed as

$$\sigma = \frac{P}{\pi R_0^2} = 2\left(\lambda_3 - \frac{1}{\lambda_3^2}\right)\left(c_1 + \frac{c_2}{\lambda_3}\right) + \frac{2\gamma_{LV}\cos\theta - \gamma_{LS}}{\sqrt{\lambda_3}R_0} - \frac{p_c}{\lambda_3} + \frac{2\gamma_{LV}\sin\theta}{\lambda_3 L}. \quad (32)$$

The above relation indicates that capillary effect can result in an additional axial load-carrying capacity of the fiber depending on the surface tension, fiber radius, axial stretch, and droplet volume. In addition, the axial engineering stress (32) can be separated into two parts: the first term is given by classic nonlinear elasticity of an axially stretched hyperelastic fiber while the other terms are the capillary contribution by the droplet. The former is independent of fiber diameter; the latter is closely related to the fiber diameter, droplet size, and contact angle.

III. NUMERICAL EXAMPLES AND DISCUSSIONS

The combined size and capillary effect in the mechanical response of axially loaded ultrathin rubbery fibers can be examined numerically according to (32). In the numerical process, material constants of the rubbery fibers c_1 and c_2 are selected to be close to those of vulcanized rubber compounds:[44] $c_1=0.2$ MPa and $c_2=0.1$ MPa. The liquid is assumed as water with $\gamma_{LV}=72.8$ dyn/cm at 20 °C. The effect of specific interface energy γ_{LS} on the mechanical behavior of thin rubbery fibers has been examined elsewhere,[40–42] and therefore is ignored herein. The numerical stress-stretch relationship of the fiber is extracted as follows. Given an axial stretch λ_3, the current fiber radius r_0 can be determined: $r_0=\lambda_1 R_0=R_0/\sqrt{\lambda_3}$. Then, the droplet volume V_0 dictates the droplet radius y_0 by solving Eq. (30) numerically. Furthermore, substituting y_0 into (29) and (31) determines the capillary pressure p_0 and droplet wetting length L, respectively. Consequently, the axial engineering stress σ can be completely determined from (32).

Figure 2 shows the stress-stretch diagrams of the thin rubbery fibers at varying R_0, θ and V_0. For the purpose of comparison, the size-independent stress-stretch diagram of the classic Mooney–Rivlin model is also plotted. During the simulations, five initial fiber radii (R_0=50, 100, 200, 500, and 1000 nm), two contact angles (θ=15° and 45°), and two dimensionless droplet volumes $[V_0/(4/3\pi R_0^3)=50, 100]$ are selected. The choice of the droplet volume guarantees formation of stable barrel-shaped morphologies according to McHale and Newton's studies.[17] Droplets wetting on hydrophobic fibers are not adopted in this study since no well-defined stable barrel-shaped droplets can be assumed on these fibers.[17]

It can be found from Fig. 2 that for given droplet volume $V_0/(4/3\pi R_0^3)$ and axial stretch λ_3, the axial stress σ increases rapidly with decreasing fiber radius R_0, i.e., droplet wetting on thin hydrophilic fibers can obviously enhance the load-

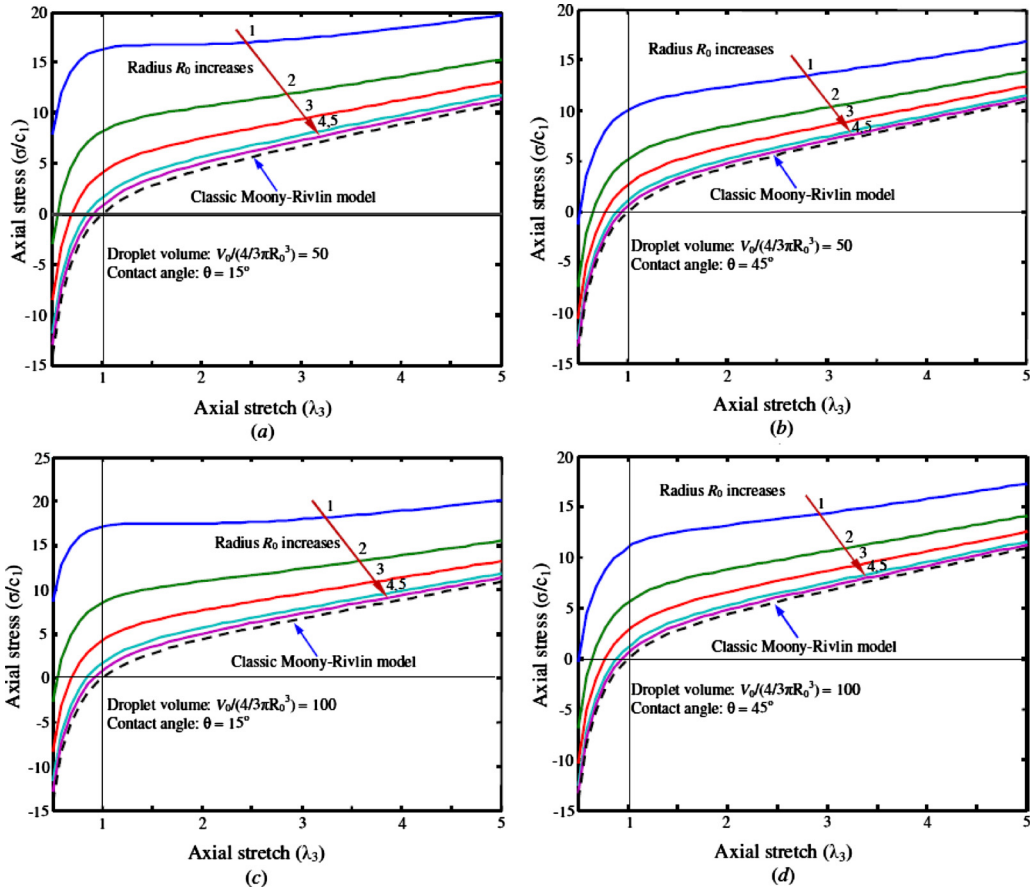

FIG. 2. (Color online) Comparison of the axial stress-stretch relationships of droplet-wetted rubbery fibers at varying initial fiber radius R_0, contact angle θ, and droplet volume V_0 with that of classic size-independent Mooney–Rivlin model. In the diagrams, indices 1, 2, 3, 4, and 5 indicate the fibers with initial radii 50 nm, 100 nm, 200 nm, 500 nm, and 1000 nm, respectively; the vertical line indicates the stretch-free state, i.e., $\lambda_3=1$.

carrying capacity of the fibers. This clearly demonstrates the combined size and capillary effect in the mechanical behavior of the ultrathin rubbery fibers. Such effect decays with increasing fiber diameter, droplet volume, and contact angle. Numerical results also show that for thin hydrophilic rubbery fibers wetted by droplets, external tensile force is required to maintain the stretch-free status (i.e., $\lambda_3=1$); the related tensile stress increases remarkably with decreasing fiber radius. In addition, effect of capillary pressure of a droplet wetting on a hydrophilic fiber can offset a part of the capillary effect exerted by the wetting fronts (compression) of the droplet. The larger is the droplet volume; the lower is the capillary pressure, i.e., the higher is the load-carrying capacity of the fiber. Furthermore, at fixed axial stress σ, wetted hydrophilic fiber segments have lower axial stretch λ_3 compared to that of the fiber segment out of the droplet. Thus, the fiber segment within the droplet is thicker than that out of the droplet due to the capillary effect.

Numerical results also indicate that contact angle has a pronounced effect on the axial stress. The axial stress σ at $\lambda_3=1$ decreases $\sim$50% when the contact angle θ increases from 15° to 45° for the thin fibers under consideration. Such effect decays with increasing axial stretch. Besides, the effect of droplet volume on the stress-stretch relationship is not significant because the capillary forces at wetting fronts dominate the mechanical behavior. In fact, the axial compression and lateral tension due to the capillary forces exerted at wetting fronts are independent of the droplet volume. By comparison with the stress-stretch diagram of the classic Mooney–Rivlin model, it can be concluded that for large fiber diameters (e.g., $R_0>1$ μm), the combined capillary and size effects on the axial stress are not significant, and therefore can be safely ignored.

In summary, relation (32) and relevant numerical results in this study have clearly demonstrated that the capillary effect has appreciable impact to the mechanical behavior of ultrathin compliant (rubbery) fibers with the diameter below 1 μm, such as those biopolymer and hydrogel nanofibers under intensive tests nowadays. These compliant nanofibers are expected to play crucial role in broad bioengineering applications such as tissue scaffolding and drug delivery, where interaction between fibers and liquids is important and commonly observed. Such an effect may further affect the elasticity, contact, and collapse of fiber networks involving droplets and vapors.[40,45–48] The present study provides an insight in understanding the hydroelastic properties of thin compliant fibers.

IV. CONCLUDING REMARKS

A hydroelastic model has been successfully formulated to examine the mechanical behavior of thin compliant fibers wetted by micro droplets. Based on classic hyperelastic Mooney–Rivlin solid model, an explicit stress-stretch rela-

tionship has been derived, which clearly demonstrates the size (i.e., fiber diameter) and capillary effects (e.g., contact angle, surface tension, and droplet volume) in the mechanical response of the droplet-on-fiber systems. At small fiber diameters, such combined size and capillary effects are noticeable, and may even trigger the elastic buckling of fibers. The results obtained in this study can be employed to guide experimental tests as well as design and analysis of compliant thin fiber-derived devices and filamentary materials involving liquid and vapor-related environments (e.g., biological, colloid and catalytic systems, ultrafine filters, etc.). The methodology presented in this study can be conveniently extended to analysis of the size and capillary effects in the mechanical response of other compliant filamentary systems.

[1]P. G. de Gennes, Rev. Mod. Phys. **57**, 827 (1985).
[2]N. R. Demarquette, Int. Mater. Rev. **48**, 247 (2003).
[3]P. G. de Gennes, F. Brochard-Wyart, and D. Quere, *Capillarity and Wetting Phenomena: Drops, Bubbles, Pearls, Waves* (Springer, New York, 2004).
[4]V. M. Starov, M. G. Velarde, and C. J. Radke, *Wetting and Spreading Dynamics* (CRC, Boca Raton, FL, 2007).
[5]D. Bonn, J. Eggers, J. Indekeu, J. Meunier, and E. Rolley, Rev. Mod. Phys. **81**, 739 (2009).
[6]M. Alava, M. Dube, and M. Rost, Adv. Phys. **53**, 83 (2004).
[7]D. Quéré, Annu. Rev. Mater. Res. **38**, 71 (2008).
[8]X. M. Chen, K. G. Kornev, Y. K. Kamath, and A. V. Neimark, Text. Res. J. **71**, 862 (2001).
[9]D. Lukas and N. Pan, Polym. Compos. **24**, 314 (2003).
[10]B. J. Carroll, J. Colloid Interface Sci. **57**, 488 (1976).
[11]H. D. Wagner, J. Appl. Phys. **67**, 1352 (1990).
[12]T. Ogawa and M. Ikeda, J. Adhes. **43**, 69 (1993).
[13]B. H. Song, A. Bismarck, R. Tahhan, and J. Springer, J. Colloid Interface Sci. **197**, 68 (1998).
[14]X. F. Wu and Y. A. Dzenis, Acta Mech. **185**, 215 (2006).
[15]www.susqu.edu/facstaff/b/vrajjer/evolver
[16]G. Mchale, M. I. Newton, and B. J. Carroll, Oil Gas Sci. Technol. **56**, 47 (2001).
[17]G. McHale and M. I. Newton, Colloids Surf., A **206**, 79 (2002).
[18]H. M. Princen, J. Colloid Interface Sci. **30**, 69 (1969).
[19]H. M. Princen, J. Colloid Interface Sci. **30**, 359 (1969).
[20]H. M. Princen, J. Colloid Interface Sci. **34**, 171 (1970).
[21]X. F. Wu, A. Bedarkar, and K. A. Vaynberg, J. Colloid Interface Sci. **341**, 326 (2010).
[22]A. Bedarkar, X. F. Wu, and A. Vaynberg, Appl. Surf. Sci. **256**, 7260 (2010).
[23]K. Keis, K. G. Kornev, A. V. Neimark, and Y. K. Kamath, in *Nanoengineered Nanofibrous Materials*, edited by S. Guceri, Y. G. Gogotsi, and V. Kuznetov (Kluwer Academic Publishers, Dordrecht, 2004), p. 175.
[24]A. Bedarkar and X. F. Wu, J. Appl. Phys. **106**, 113527 (2009).
[25]A. Virozub, N. Haimovich, and S. Brandon, Langmuir **25**, 12837 (2009).
[26]D. H. Reneker and I. Chun, Nanotechnology **7**, 216 (1996).
[27]D. H. Reneker, A. L. Yarin, E. Zussman, and H. Xu, Adv. Appl. Mech. **41**, 43 (2007).
[28]Y. Dzenis, Science **304**, 1917 (2004).
[29]D. Li and Y. N. Xia, Adv. Mater. (Weinheim, Ger.) **16**, 1151 (2004).
[30]Z. M. Huang, Y. Z. Zhang, M. Kotaki, and S. Ramakrishna, Compos. Sci. Technol. **63**, 2223 (2003).
[31]H. Yokoi, T. Kinoshita, and S. G. Zhang, Proc. Natl. Acad. Sci. U.S.A. **102**, 8414 (2005).
[32]H. Q. Liu, M. Zhen, and R. H. Wu, Macromol. Chem. Phys. **208**, 874 (2007).
[33]C. Y. Tang, S. H. Ye, and H. Q. Liu, Polymer **48**, 4482 (2007).
[34]J. W. Xie, X. R. Li, and Y. N. Xia, Macromol. Rapid Commun. **29**, 1775 (2008).
[35]S. Koutsopoulos, L. D. Unsworth, Y. Nagaia, and S. G. Zhang, Proc. Natl. Acad. Sci. U.S.A. **106**, 4623 (2009).
[36]S. G. Cao, B. H. Hu, and H. Q. Liu, Polym. Int. **58**, 545 (2009).
[37]J. M. Gere, *Mechanics of Materials* (Books/Cole, Pacific Grove, CA, 2001).
[38]R. W. Ogden, *Non-Linear Elastic Deformation* (Dover, New York, NY, 1997).
[39]W. M. Lai, D. Rubin, and E. Krempl, *Introduction to Continuum Mechanics* (Butterworth-Hernemann, Woburn, 1993).
[40]X. F. Wu and Y. A. Dzenis, J. Appl. Phys. **102**, 044306 (2007).
[41]X. F. Wu, Y. Y. Kostogorova-Beller, A. V. Goponenko, H. Q. Hou, and Y. A. Dzenis, Phys. Rev. E **78**, 061804 (2008).
[42]X. F. Wu, J. Appl. Phys. **107**, 013509 (2010).
[43]S. C. Cowin and S. B. Doty, *Tissue Mechanics* (Springer, New York, 2007).
[44]L. T. G. Trelorar, *The Physics of Rubber Elasticity* (Clarendon, Oxford, 1975).
[45]X. F. Wu and Y. A. Dzenis, J. Appl. Phys. **98**, 093501 (2005).
[46]X. F. Wu and Y. A. Dzenis, J. Appl. Phys. **100**, 124318 (2006).
[47]X. F. Wu and Y. A. Dzenis, Nanotechnology **18**, 285702 (2007).
[48]X. F. Wu and Y. A. Dzenis, J. Phys. D: Appl. Phys. **40**, 4276 (2007).